A pulsed ‘plasma broom’ for dusting off surfaces on Mars

2017 New J. Phys. 19 063006

(http://iopscience.iop.org/1367-2630/19/6/063006)

New Journal of Physics
The open access journal at the forefront of physics

Deutsche Physikalische Gesellschaft DPG
IOP Institute of Physics

Published in partnership with: Deutsche Physikalische Gesellschaft and the Institute of Physics

OPEN ACCESS

RECEIVED
21 September 2016

REVISED
3 February 2017

ACCEPTED FOR PUBLICATION
16 February 2017

PUBLISHED
5 June 2017

PAPER

A pulsed 'plasma broom' for dusting off surfaces on Mars

C M Ticoş, A Scurtu and D Ticoş

National Institute for Laser, Plasma and Radiation Physics, 077125 Bucharest, Romania

E-mail: catalin.ticos@inflpr.ro

Keywords: plasma jet, dusty surface, Mars

Abstract

Dust is a challenge for the design and operation of equipment on the Martian surface, particularly for solar cells. An efficient and robust technique for removing dust and sand from surfaces immersed in CO_2 at low pressure is presented. The working principle is based on a pulsed plasma jet produced between two coaxial electrodes biased at voltages between 1 and 2 kV. A demonstration is presented using dust particles whose chemical composition mimic the Mars soil. An array of connected photovoltaic cells fully covered with dust and sand is exposed to the plasma jet. The cells open circuit voltage is monitored in real-time thus providing the means to measure the dust removal efficiency. A good cleaning efficiency is attained after a few shots in a geometry where the plasma jet is directed perpendicularly to the dusty surface. The main advantage of this approach lies in the opportunity to apply it directly at about 5 Torr, the pressure of the Martian environment. A numerical evaluation shows that the plasma drag force on a dust particle is orders of magnitude higher than its weight depending on plasma density and flow speed, hence validating the principles of this cleaning technique.

1. Introduction

Fine dust particles are ubiquitous on Mars [1]. Storms or light winds can blow dust up in the atmosphere and carry it over large distances. When the lifting force of the wind ceases the dust particles settle down and deposit as a fine layer [2]. The dust particles can range in size from a fraction of a micron to several tens or hundreds of microns [3]. Larger sand particles ($\gtrsim$1 mm) are transported by saltation when the wind shear velocity reaches a threshold value of a few m s^{-1} at the ground level [4]. The chemical composition of the dust and sand particles varies depending on their location. It consists predominantly of silicates and metallic oxides (SiO_2, Al_2O_3, FeO, Fe_2O_3, MgO and CaO) [5]. A type of regolith with a similar chemical composition and made of volcanic ash with particle sizes up to 1 mm known as JSC Mars-1A can simulate the Martian dust [6].

Planners of future missions to Mars have acknowledged that dust presence and its accumulation can be a nuisance for several reasons [7]. It can render optical detectors or cameras inoperable by covering their view or it can decrease the power production of solar panels by blocking the Sun rays at a rate $\approx$0.3% per day [8, 9]. Photographs taken by probes placed on Mars often showed a fine dust layer covering the surface of their solar panels. Moreover, dust and sand can penetrate through holes and slits and reach the bearings, joints and movable parts of tools or equipment and induce unwanted frictional forces [10]. Last but not least dust can be a potential treat for human health by inhalation if it is present inside the human habitat [11].

1.1. Dust removal on Mars

The fine dust particles are highly adherent to surfaces due to a combination of factors, such as electrification [12] (due to a high flux of UV radiation and low content of water vapors in the atmosphere or due to high electric fields during storms) and chemical composition (e.g. dust with a high ferric content is easily magnetized) [13]. In order to solve this dust contamination problem several approaches have been proposed each with its own benefits and disadvantages [14–22]. The cleaning efficiency varies largely depending on several factors, from the type of dust removal mechanism (electrical or mechanical) to its implementation and operation. Electrical

approaches are contactless while mechanical ones seem to be affected by the triboelectric effect, the inherent charging of the dust particles by friction. In the first category an established dust removal technique consists in printing directly on the surface (insulating or dielectric) an electrostatic shield made of a fine conducting mesh-grid [18–20]. When charged dust particles adhere to the surface a high voltage is applied on the grid wires and the electrostatic force repels them off. The removal process takes a relatively long time, from minutes to several hours for an efficient surface cleaning. A second solution consists in the use of a precipitator to collect dust during the process of extracting oxygen, water or methane from the Martian atmosphere [21]. A tube provided with two electrodes produces a corona discharge when a high voltage is applied. The electric field drives electrostatically the charged dust to one electrode where it is trapped. Both methods become less efficient when the surface is covered with a thick layer of dust, and particularly for larger particles (e.g. in the mm range) for which electrical levitation becomes questionable due to the particles weight. It appears that lifting off large particles with electric fields is a major challenge of the electrical removal techniques.

1.2. Surface cleaning by plasma jet

In order to overcome this deficiency we propose a much more robust cleaning technique which seems to be very effective for a wide range of particle diameters (from microns to 1 mm and even beyond this size, thus including sand particles) and much more rapid compared to known methods. The removal of dust is based on a plasma jet produced in a pulsed discharge. A proof-of-principles demonstration is presented in the followings, by cleaning an array of PV cells heavily covered with dust and sand immersed in CO_2 at low pressure.

Mars atmosphere is composed mainly of CO_2 (95%), N_2 and Ar in small percentage (2.7% and 1.6%, respectively) and traces of O_2 and CO (each below 0.2%) [23]. The atmospheric pressure at the planet surface varies between 3.5 and 7.5 Torr. Even at the reduced atmospheric pressure of the environment dust is susceptible to the drag force of the wind. The drag force exerted by a flowing gas on a small spherical dust grain is the well known Stoke formula $F_{gas} = 6\pi\rho\nu r_d v_g$ proportional to the gas density ρ and its kinematic viscosity ν, sphere radius r_d and gas flow speed v_g relative to the grain. By equating it with the weight of the particle $m_d g$ one obtains a first order estimate of the threshold speed for detaching a grain from a surface. A more rigorous approach takes into consideration the adhesion force and the effect of the surface roughness [3, 4].

It is conceivable that if dust is transported and deposited by the force of wind gusts, it can also be removed from a surface by the same physical process. In fact self-cleaning of dust from solar panels and surfaces of rovers cruising on the surface of Mars has been well documented in numerous photographs. Such a phenomenon is called *cleaning event* [24]. Removal of dust from a surface by blowing gas can be effective if two conditions are met, according to the above formula: the speed and the density of the flowing gas are large enough to provide a strong lift off force to the microparticles. Such studies have been conducted in gas at low pressure similar to the Martian atmosphere [4]. At sub-atmospheric pressure a viable alternative to a gas jet is to produce a plasma jet by ionizing the static gas and accelerating it in an electric field. Our proposed cleaning method is based on this feature. The advantages of such a technique are multiple: the gas at the ambient low pressure is accelerated to supersonic speed (at several km s^{-1}) thus eliminating the need for compressed gas at high pressure, and since the pulsed discharge lasts for a short time (sub-millisecond) the drag force exerted by the plasma (the rate of momentum transfer) is high.

A typical device for producing dense pulsed plasma jets is the coaxial plasma gun. Plasmas produced between coaxial electrodes have been intensely investigated beginning with the late 60's with the goal of obtaining surplus energy from fusion reactions [25]. Later, their potential application in space propulsion has been recognized due to their high ion density and ejection speed resulting in a high thrust force [26]. In light of the new ambitions for human space exploration the interest for this type of discharge has been renewed recently since the magnetoplasmadynamic accelerator is one the most powerful form of electric propulsion [27]. The plasma wind force has been exploited in fusion applications related to the acceleration of microparticles to hypervelocities [28] or in removing dust floating inside a plasma reactor [29]. Hypervelocity dust particles can be used as a tool for diagnozing hot plasmas [30] or for quenching instabilities in tokamak plasmas [31].

2. Method and materials

A coaxial gun producing a plasma jet is shown schematically in figure 1. It is composed of two metallic electrodes, an inner rod and an outer cylindrical shell. The two electrodes are made of stainless steel, a center rod with 6 mm in diameter and a cylinder with 17 mm inner diameter. The length of the coaxial gap is 64.5 mm. The gun was powered by a charged capacitor ($C = 500\ \mu$F) triggered by closing a Ross high current (12 kV, 50 kA pulsed) electromagnetic switch. In our technique the coaxial gap was filled with pure CO_2 at the low ambient pressure of the vacuum chamber of a few torr and an electrical discharge was initiated by applying a high voltage on the electrodes. The radial applied electric field induces the current $\boldsymbol{J}$ between the electrodes, composed of the

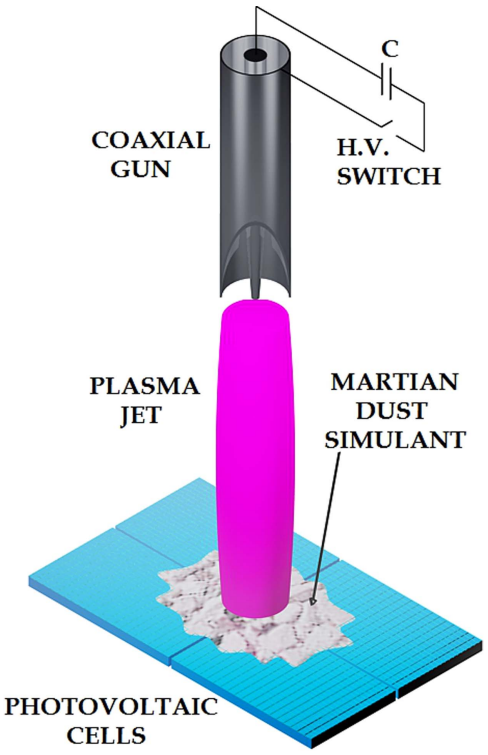

Figure 1. Experimental set-up and cut in the coaxial gun showing the inner electrode; the expelled plasma jet is aimed perpendicularly at an array of PV cells covered with JSC Mars-1A.

flowing electrical charges (ions and electrons) of the plasma. The electrical current passing trough the inner rod generates a toroidal magnetic field $\boldsymbol{B}$. The product $\boldsymbol{J} \times \boldsymbol{B}$ is the Lorentz force which accelerates axially the plasma and ejects it out of the gun. The speed and density of the plasma flow is directly dependent on the energy supplied into the discharge. The discharge current was measured with a Rogowski coil (with a conversion factor 1 V per 100 A) and 2 attenuators (20 and 3 dB).

For our electrode geometry the Paschen breakdown occurred at about 650 V at 5 Torr. From the point of view of the electrical discharge the breakdown voltage in the presence of pure CO_2 should not differ significantly from the case of a Martian mixture of gases as demonstrated in [32]. The same with the polarity of the electrodes, which does not seem to influence the initiation of the discharge. In the case of coaxial electrodes made of stainless steel the lowest value of the Paschen curve is situated between 200 and 275 V for values of the product between the gas pressure and the radius of the inner electrode in the range 0.03–0.08 Torr cm [33].

The plasma density and temperature were measured with a triple Langmuir probe [34, 35]. It consisted of three identical probe tips made of a tungsten wire with a diameter 0.6 mm and length 4.5 mm inserted axially within the plasma jet at a distance of 4 cm. A constant DC voltage (from 5 to 50 V) was applied between probes #1 and #3 while the currents picked up by these probes ($I_1 = -I_3$) were measured with Rogowski coils (1 V per 1 A). The voltage $V_{\rm dif}$ between the floating probe #2 and the biased probe #1 was measured with a differential voltage amplifier. The electron temperature is deduced from the following equation [35]:

$$k_B T_{\rm e} = \frac{V_{\rm dif}}{\ln(2)}. \tag{1}$$

The ion saturation current to the probe tips is given by the equation:

$$I_+ = I_1 \frac{\exp\left(-\frac{eV_{\rm dif}}{k_B T_{\rm e}}\right)}{1 - \exp\left(-\frac{eV_{\rm dif}}{k_B T_{\rm e}}\right)}, \tag{2}$$

while the electron density in the plasma is a function of the saturation current I_+ and the electron temperature $k_B T_{\rm e}$:

$$n_{\rm e} = \frac{I_+}{\exp\left(-\frac{1}{2}\right) e A_+ \sqrt{\frac{k_B T_{\rm e}}{m_{\rm i}}}}, \tag{3}$$

where $m_{\rm i}$ is the mass of the ion (CO_2^+), and A_+ is the ion collection area or surface of the probe.

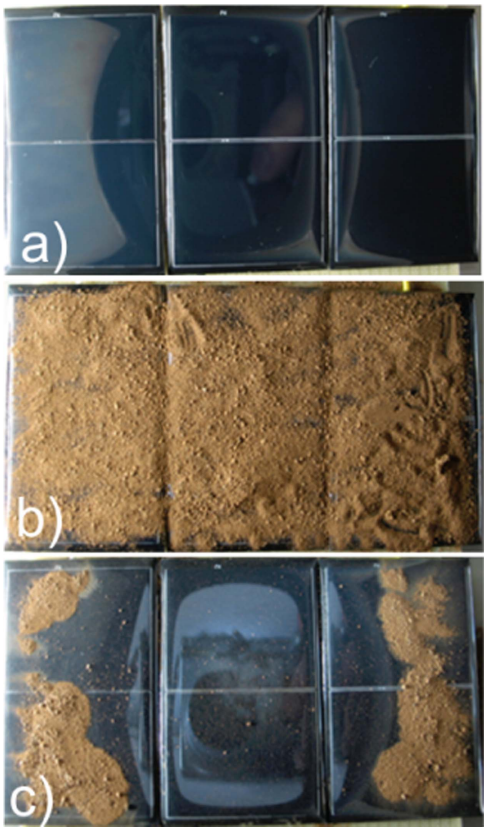

Figure 2. Top view of an array of three PV cells with a total area 83 cm^2 connected in series: (a) no dust present; (b) fully covered with dust and sand; (c) partially cleaned after 20 shots at 1 kV. The PV cells were photographed after opening the vacuum chamber and removing the coaxial gun.

High quality identical PV cells were positioned horizontally in the vacuum chamber at a varying distance from the coaxial gun muzzle, as shown in figure 1. The cells (model # SMH 2-0480) were monocrystalline (c-Si) and covered with Polyurethane. They had an area 27.68 cm^2 (the exact size was 67.5 $\times$ 41 mm^2 and thickness 1.8 mm). Their open circuit voltage was 1.32 V in standard test conditions. Either one cell or an array of three cells positioned next to each other, as shown in figure 2(a), were tested independently. The cells were illuminated through the side viewport of the vacuum chamber by a photographic lamp with 48 LEDs disposed circularly on a ring and delivering a luminous flux of 10 lm/LED. The average illuminance of the PV cells was 1245 lx. The photographic lamp used to illuminate the dusty or clean PV cells had a diameter of 10 cm and it was placed at 6 cm from the first cell outside the vacuum chamber. A 99% optical transmission was taken for the glass viewing port of the chamber. Only the upper half of the lamps LEDs were actually situated above the plane of the cells and contributed to the incident light falling upon the cells surface. The illuminance was 2460 lx for the cell closest to the lamp, 880 lx for the mid cell and 400 lx for the farthest cell.

The JSC-Mars 1A Mars simulant is a brown powder obtained from volcanic ash and made up of particles with sizes from a few microns up to 1 mm, as shown in figure 3(a). More details concerning the irregular shape of the smallest particles are provided in figure 3(b) obtained with a scanning electron microscope (SEM). Its chemical composition inferred by energy dispersive x-ray analysis (EDS) shows a high content of O_2 (42.5%), C (16.2%), Al and Si in the same proportion (11.8%) and Fe (11.3%). A low content of Ca (2.2%) and Ti (1.8%) is found, while there are traces of Mg, Na and Mn (~0.45% and ~0.4%, respectively). These results are in good agreement with the analysis presented by Allen *et al* [6] where the main identified compounds are SiO_2 (43.5%), Al_2O_3 (23.3%), Fe_2O_3 (15.6%), CaO (6.2%), TiO_2 (3.8%), and MgO (3.4%) . The grain size distribution given in table 1. is not uniform: the larger particles of a few hundred microns are prevailing. The mass density of JSC Mars-1A is $\rho = 1.91\ g\ cm^{-3}$ [6].

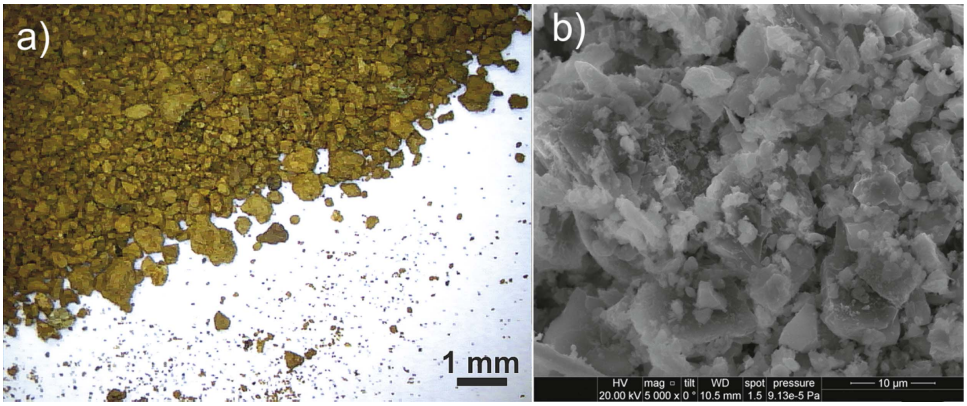

Figure 3. (a) Image of dust simulant JSC Mars-1A showing particles as small as 10 μm (the smallest visible dots) and as large as 1 mm; (b) zoom-in image with size 52.5 $\times$ 45.5 μm obtained with a SEM.

Table 1. Grain size distribution, from [6].

Size (μm)	<5	5–52	53–149	150–249	250–449	450–1000
Weight (%)	1	5	19	24	30	21

3. Results and discussion

3.1. Cleaning efficiency on PV cells

The open circuit voltage of the clean PV cells was $V_{oc0}^{(1/2)} = 0.3$ V when illuminating half a cell, $V_{oc0}^{(1)} = 0.6$ V for one full cell, whereas for the array of all three cells connected in series $V_{oc0}^{(3)} = 1.4$ V. The cells were then thoroughly covered with a 1 mm layer of Martian simulant JSC Mars-1A as shown in figure 2(b) blocking completely the incident light on the cells, and insuring that $V_{oc0}^{(i)} = 0$ V with $i = 1/2$, 1 and 3, respectively. The coaxial gun was mounted vertically, and centered above the cells depending on their arrangement. When operating with half a cell the other half was masked by an opaque tape. When operating with the full cell the coaxial gun was pointing towards the cell center while for the case of the three-cell array it was centered above the mid-cell. The coaxial gun was fired successively at regular time intervals of about 2 min, leaving sufficient time for charging up the capacitor. The voltage delivered by the individual cell or the cell array was monitored continuously and measured after each shot. The cleaning efficiency was inferred as the ratio $E^{(i)} = V_{oc(dusty)}^{(i)} / V_{oc_0}^{(i)} \times 100(\%)$ after a series of shots, where $V_{oc(dusty)}^{(i)}$ is the voltage of the cell or of the cell array ($i = 1/2$, 1 and 3, respectively) with dust on its surface. The results are shown in figures 4(a)–(c) where measurements have been carried out for a half cell, a single cell and an array of three connected cells, respectively.

The results for a single shot are as follows: $E^{(1/2)} = 37\%$–18% (figure 4 (a)) and $E^{(1)} = 18\%$–15% (figure 4 (b)) for the range of distances between 5 and 11.5 cm, respectively. At an intermediate distance of the above range, i.e. at 9 cm, $E^{(3)} = 20\%$ (figure 4(c)). After a few shots and at the closest distances, between 5 and 9 cm, $E^{(1/2)} \approx 99\%$ which means that a total cleaning was rapidly obtained. For obtaining the same cleaning efficiency at 11.5 cm, 16 shots were required. We note that the number of shots increases exponentially with distance in order to obtain a complete surface cleaning. For the single cell $E^{(1)} \approx 99\%$ after 6 to 8 shots at a distance between 5 and 9 cm, while at 11.5 cm about 18 shots were needed. In the case of three cells the efficiency increases slowly with the number of shots at distances of 8 and 9 cm, reaching a saturation value $E^{(3)} = 80\%$ after 20 shots. The partial cleaning obtained in the setup with three cells is expected as the side cells were not directly exposed to the plasma jet. However, the shock wave produced by the fast propagating plasma jet is reflected along the surface of the cells and entrained the dust particles in a sideways motion.

3.2. Cleaning efficiency by weighing dust

An alternative method for inferring the cleaning efficiency consists in weighing pre- and post-plasma exposure some samples whose surfaces were covered with dust. The coaxial gun muzzle was placed 1 cm far from each sample and the center axis of the plasma jet was at about 1.5 cm from the surface. In this case the plasma jet was parallel with the surface [36]. Several identical plates made of glossy cardboard with an area 29.61 cm^2 (51.5 $\times$ 57.5 mm^2) were fully covered with dust simulant JSC Mars-1A. The mass of a cardboard plate was

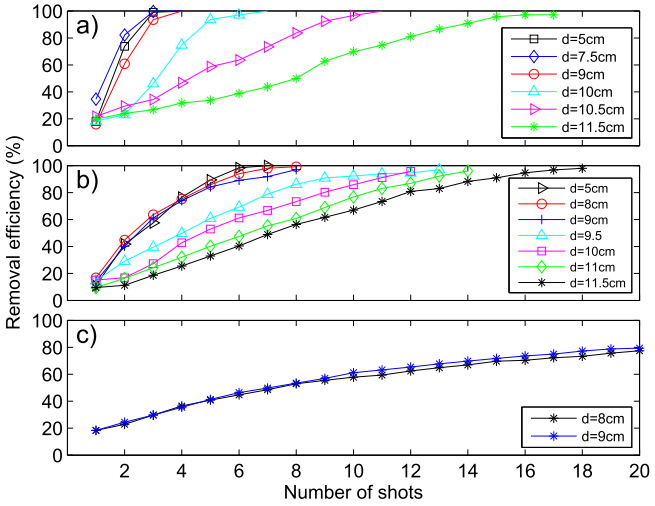

Figure 4. (a) Cleaning efficiency depending on the distance between the coaxial gun and cells surface: (a) for a half PV cell; (b) for one full cell; (c) for three cells positioned next to each other as shown in figure 2.

Table 2. Cleaning efficiency E (%) of a dusty cardboard surface depending on the number of shots at 1, 1.5 and 2 kV, respectively.

Voltage (kV)	Number of shots				
	1	2	3	4	5
1	14.4%	27.2%	39.2%	49.3%	64.3%
1.5	21.5%	45.2%	56.0%	61.6%	80.2%
2	82.3%	90.1%	97.0%	na	na

1.1772 g. The mass of dust deposited on a sample varied between 0.4997 and 0.6029 g. The mass measurements were carried out with a high precision balance having an accuracy 10^{-4} g.

The use of the glossy cardboard demonstrates that the technique works with other types of surfaces as well and it gives an indication of the precise dust quantity that can be removed. Weight measurements with this accuracy are possible only within some limited mass ranges allowed by the high precision balance. The cardboard sheets are light whereas the PV cells are two heavy compared with the dust deposited on their surface.

The cleaning efficiency was measured considering the total weight of each sample including that of the dust: $E = [1 - (M_{\text{dusty}} - M_{\text{clean}})/M_{\text{dust}}] \times 100$ (%), where M_{dusty} and M_{clean} are the masses of the sample with and without dust, respectively, and M_{dust} is the initial mass of dust on the sample.

At 1 kV E increases with roughly 10%–15% per shot, as shown in table 2. At 2 kV the first shot achieved $E = 82.3\%$, while for the next two shots E increased by $\approx$7%. It should be noted that at 2 kV the released energy into the discharge is larger by a factor of 4 compared to the 1 kV shot. For 1.5 kV shots the efficiencies are approximately in-between those obtained at 1 and 2 kV.

One important feature of this cleaning technique is the use of a high voltage in the few kV range (only 1–2 kV) which implicitly requires a relatively low amount of stored energy. At 1 kV the 500 μF capacitor stored 250 J and given the peak value of the pulsed current obtained, the corresponding peak power was 7 MW. The goal was to use as little energy as possible and the trade-off is between choosing the charging voltage of the capacitor (or energy level) and the generation of sufficiently high discharge current at a given gas pressure in order to produce enough plasma thrust for pushing the dust particles.

Coaxial guns are known for electrode sputtering due to the high radial electric fields. An additional benefit of working at 1 kV is keeping the sputtered material at low levels as we found no significant contamination on the surface of the PV cells after many shots. It should be pointed out however that contamination due to electrode erosion is less of an issue for surfaces covered with a thick layer of dust since the detached material from the gun electrodes collides first with the dust particles, and thereafter with the surface.

Another aspect is that the electromagnetic noise associated with the flowing pulsed currents of only a few kA did not interfere with the proper functioning of the PV cells or other pieces of electronic equipment nearby. Cleaning of the solar panels can be achieved by mounting the coaxial plasma gun on a mobile robotic arm. Firing

the plasma jet at an angle could guide the ejected dust along a controlled direction until all dust particles would eventually be pushed out of the cells surface.

3.3. Cleaning effectiveness (CE)

A comparison between surfaces with different areas and having different cleaning efficiencies is not straightforward, as is the case of the PV cells and the cardboard sample used in the experiment. In order to make such a quantitative evaluation a new physical quantity is introduced: *the CE* which is defined as the cleaning efficiency multiplied by the area of the cleaned surface: $\mathrm{CE} = E(\%) \cdot 10^{-2} \cdot S$ (cm^2). Basically, CE is the same when cleaning two different areas with 1 cm^2 and 2 cm^2 but with 100% and 50% efficiency, respectively.

The cleaning effectiveness is evaluated in the case of three consecutive shots (of figure 4) for half a PV cell, one full cell and three connected cells at 1 kV and 9 cm distance: CE = 12.5, 16.3 and 23.8% cm^2, respectively. In the cases of the cardboard sample (for 1, 1.5 and 2 kV) the three consecutive shots produce the following values: CE = 11.6, 16.6 and 29.6% cm^2, respectively. One can see that at 1 kV half of the PV cell (E = 93.5% and $S = 13.34$ cm^2) is more effectively cleaned than the cardboard sample (E = 39.2% and $S = 29.61$ cm^2). On the other hand, the cardboard sample is roughly as effectively cleaned at 1.5 kV (E = 61.2% and $S = 29.61$ cm^2) as one full PV cell at 1 kV (E = 56.0% and $S = 26.68$ cm^2).

Differences in the cleaning efficiencies can arise from the tribological properties of the surface. A direct determination of the friction coefficient has been carried out using a standard CSM ball-on-disc tribometer equipped with a 6 mm diameter saphire ball and set at 0.25 N applied force: for the PV cell $\mu_{\mathrm{PV}} = 0.19 \pm 0.02$ and for the glossy cardboard sample $\mu_{\mathrm{cardboard}} = 0.04 \pm 0.01$.

3.4. Energy budget for cleaning operation

In order to asses the validity of this proposed cleaning technique from an energy budget point of view, an estimate of the consumed energy for cleaning a given area relative to the solar energy produced by the same area is evaluated. We consider here solar cells with an area 83 cm^2, similar with that of the three connected PV cells of our experiment. The total peak irradiance at the surface of Mars varies largely depending on sun elevation, amount of dust in the atmosphere, seasonal variation and direct and diffusive irradiation. An average value is however provided by Haberle *et al* in [37] for the Viking Lander 1 site: 3 kW h m^{-2} per day. With state of the art triple junction GaAs solar cells having a 30% efficiency, as those produced for space applications, a total electrical solar power of 900 W h m^{-2} per day can be obtained, which is equivalent to 3.24 MJ m^{-2} or 324 J cm^{-2}. A PV array with an area 83 cm^2 would therefore produce 26.9 kJ daily. If 20 shots will be used to clean this array then 5 kJ will be needed (at 250 J per shot corresponding to 1 kV shots) which represents about 18.6% of the daily energy production rate. With this amount of energy only 5 shots will be possible at 2 kV, but in this case the removal efficiency is also higher. The operation of the coaxial gun seems therefore feasible. However this situation is not encountered often because strong dust storms which would completely burry the solar cells in sand are not produced on a daily base, and therefore a thorough cleaning of the solar cells would be performed once every period.

3.5. Plasma diagnostics

The operation of our coaxial gun with prefilled gas at a few torr can be well described by the snow plow model [38]. In this approach a thin plasma sheath is formed at the back of the electrodes and travels along the gun axis as an ionization shock waves towards the front end of the gun. Numerical simulations carried out for the parameters of our experiment have produced results consistent with the measurements, i.e. the plasma plume speed in the range of 1–5 km s^{-1} and peak discharge currents of 6–12 kA [39]. This regime is different from the deflagration operation mode induced by puffing gas inside the coaxial gap with electrodes biased at tens of kV [40].

In order to characterize the ejected plasma the speed of the plume has been imaged with an ICCD camera. Figure 5 shows the sequence of images (a)–(f) recorded at different moments from the time zero of the discharge current. The average plasma plume speed was 1.4 ± 0.2 km s^{-1} obtained at 1 kV and 5 Torr, and is a factor of 5 larger than the sound speed in CO_2 (~285 m s^{-1}). For 1.5 kV the speed of the plasma jet was 1.6 ± 0.3 km s^{-1} while at 2 kV it was 1.9 ± 0.3 km s^{-1}. The rapidly expelled plasma jet from the gun nozzle shown in figures 5(a) and (b) is pushing against the inert gas and creates a shock wave observed in figures 5(c) and (d). The shock wave is moving axially and expands transversally as seen in the images (e) and (f) of figure 5. It is the collision of the shock wave and its sideways expansion that impinges upon the dust particles situated on the PV cells at several centimeters from the gun axis. However, the dust which is relatively far positioned and interacts little with the plasma is not affected and stays on the surface as seen in figure 2(c) where a dust layer in the shape of a ring is not removed.

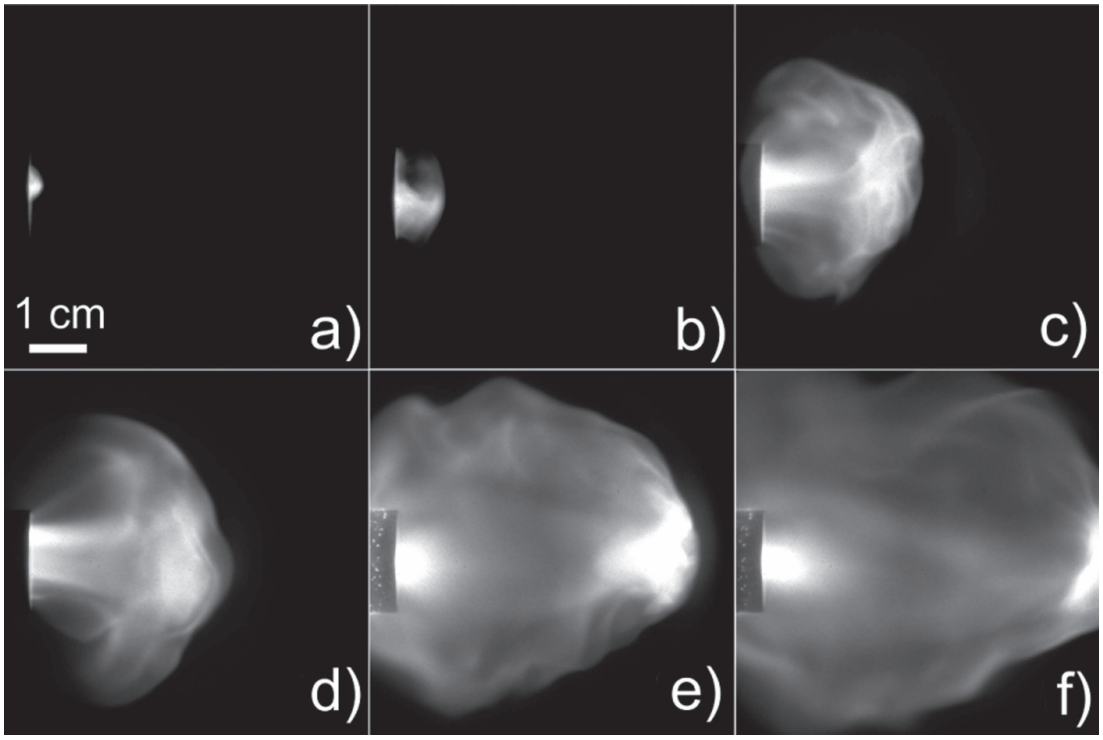

Figure 5. (a) Plasma jet exiting the coaxial gun muzzle; (b)–(f) plasma jet expanding in CO_2 at 5 Torr. The images in (a)–(f) had an exposure of 0.5 μs and were acquired from time zero of the discharge current rise at 46.5 μs, 57.1 μs, 66.2 μs, 75.0 μs, 84.7 μs, and 94.8 μs, respectively.

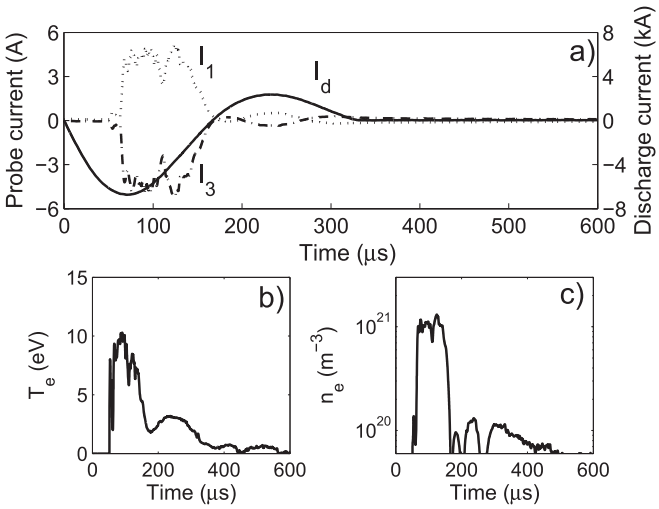

Figure 6. A 1 kV plasma shot: (a) discharge current I_d and triple-probe currents I_1 and I_3 mirroring each other; (b) electron temperature; (c) electron density.

In the pressure range 1–5 Torr the discharge current had a peak value of 7 kA at 1 kV and 14 kA at 2 kV, while the discharge period was approximately 350 μs, as shown in figure 6(a). The peak electron temperature was found to be $T_e \simeq$ 10–12 eV while the peak electron density was $n_e \simeq 7 \times 10^{20}$ m^{-3}–10^{21} m^{-3} for 1 kV shots, as shown in figures 6(b) and (c), respectively. In the case of 2 kV shots $T_e \simeq$ 11–14 eV, while $n_e \simeq 10^{21}$ -2×10^{21} m^{-3}. For shots at 1.5 kV $T_e \simeq$ 10–13 eV, and $n_e \simeq 9 \times 10^{20}$ -1.5×10^{21} m^{-3}. While the ion temperature has not been measured, it is supposed that the ions are cold ($T_i \ll 1$ eV) and the ion heat flux to the surface is negligible. The mean free path of CO_2 molecules at 5 Torr is $\approx$12 μm while the Debye length for the measured plasma parameters is $\lambda_D \approx$ 0.6–0.9 μm.

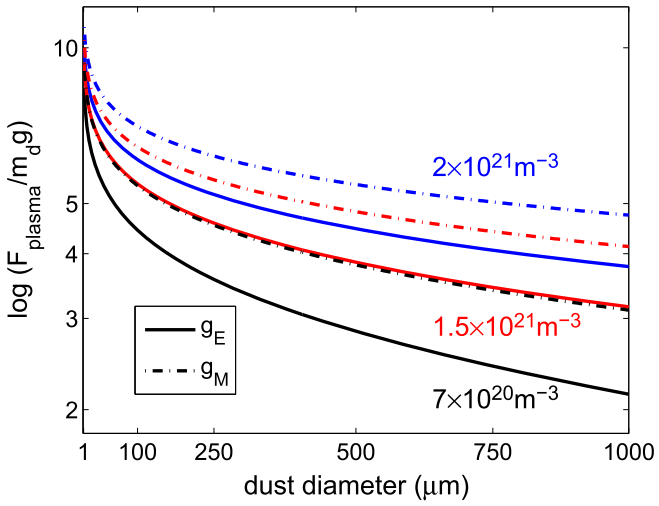

Figure 7. Logarithm of the plasma wind force relative to the weight of a spherical dust particle for the gravitational accelerations on Earth ($g_E = 9.81$ m s^{-2} with continuous line) and Mars ($g_M = 3.71$ m s^{-2} with dotted line), and for the following values of the plasma density $n_e = 7 \times 10^{20}$ m^{-3} (black curves), 1.5×10^{21} m^{-3} (red curves) and 2×10^{21} m^{-3} (blue curves), corresponding to shots at 1 1.5 and 2 kV, respectively.

3.6. Plasma drag force on a dust particle

The plasma drag force exerted on a spherical dust particle by an ionized gas is [28, 41]:

$$F_{\text{plasma}} = 2\pi r_d^2 k_B T_i n_i G_0(s), \tag{4}$$

where

$$G_0(s) = \left(s^2 + 1 - \frac{1}{4s^2}\right)\text{erf}(s) + \left(s + \frac{1}{2s}\right)\frac{\exp(-s^2)}{\sqrt{\pi}}$$

and

$$s = \sqrt{\frac{m_i v_p^2}{2k_B T_i}},$$

$k_B T_i$ is the ion temperature (in our case $T_i = 0.025$ eV), n_i is the ion density ($n_i = n_e$), and v_p is the plasma jet speed. The force is numerically simulated and shown in figure 7. It takes into account the collisional ion drag which depends on the plasma jet speed, the plasma density and the dust radius and mass. Since the dust particles are much larger than the plasma screening length ($r_d \gg \lambda_D$) the orbital ion drag force which arises from the long range Coulomb interactions of ions with a charged dust particle is neglected [42]. In fact $\lambda_D < 1$ μm and $r_d \geqslant 5$ μm for 99% of the dust inventory, as shown in table 1.

The plasma drag force F_{plasma} relative to the dust weight $m_d g$ is evaluated for the following plasma jet densities: $n_i = 7 \times 10^{20}$, 1.5×10^{21} and 2×10^{21} m^{-3}. Also the dust weight has been considered on Earth and on Mars where the gravitational acceleration is about 2.6 times lower.

On Earth, for the smallest dust particle with a diameter of 1 μm $F_{\text{plasma}}/m_d g$ is $\approx 10^8$ and $\approx 10^{10}$ for the lowest and highest plasma densities considered, respectively. As the diameter of the dust grain increases up to 1 mm, the ratio of forces drops quickly to $\approx 1.4 \times 10^2$ and $\approx 6.3 \times 10^3$, for the two cases. On Mars however, dust lift off by the plasma drag force seems to be much more effective. At the lowest plasma density and for the 1 mm dust grain, the plasma drag force is over 3 orders of magnitude higher then its weight ($\approx 10^3$), while at the highest plasma density this ratio goes to $\approx 5.6 \times 10^4$. At the same time, for the 1 μm dust grain the force ratio is between $\approx 10^9$ and 10^{11}, for these two plasma densities. Similar drag force ratios are observed when comparing the following two cases: the lowest plasma density (i.e. 7×10^{20} m^{-3}) and Mars gravity with the mid-value plasma density (i.e. 1.5×10^{21} m^{-3}) and Earth gravity. As a general remark we can assert that the plasma wind force is many orders of magnitude larger than the dust weight in all discharge conditions that we tested, while for the largest dust grains it is sufficiently high in order to achieve a good surface cleaning.

4. Conclusions

In an attempt to imitate the natural cleaning of surfaces on Mars by winds with a speed in the few m s^{-1} range, we propose a robust technique for dusting off surfaces using a pulsed plasma jet which features a plasma wind speed

3 orders of magnitude higher, in the km s^{-1} range. The plasma was created in a discharge with two electrodes having a coaxial geometry in a miniature configuration of a few centimeters in size, at the pressure of the Martian atmosphere. Among the obvious advantages of this new method is the efficient cleaning of any type of surfaces with different morphology including those of solar cells, only after a few shots. The gun was operated at voltages between 1 and 2 kV in order to minimize the required energy per pulse and a demonstration on a dusty set of PV cells was carried out using only 250 J per pulse. Diagnostics of the pulsed plasma jet using a Langmuir triple probe and a high speed ICCD were carried out for inferring the plasma density and temperature and the plasma flow speed. The plasma drag force acting on the dust particles is numerically evaluated using a model for ion collection on the dust surface by direct impact collisions. An EDS chemical characterization of the JSC-Mars-1A dust simulant was carried out while details about the size and shape of the particles were obtained in a microscopic image obtained with a SEM.

Acknowledgments

The authors acknowledge financial support from the Romanian Space Agency (ROSA) from Contract #100 within the Space Technology and Advanced Research (STAR) competition C2-2013. We would like to thank Dr C Poroşnicu and Dr O Pompilian for helping with the measurement of the friction coefficient using the tribometer.

References

[1] Team R 1997 Characterization of the Martian surface deposits by the Mars Pathfinder Rover, Sojourner *Science* **278** 1765
[2] Carr M H 2007 *The Surface of Mars* (Cambridge: Cambridge University Press) p 194
[3] Greeley R and Iversen J D 1985 *Wind as a Geological Process on Earth, Mars, Venus and Titan* (Cambridge: Cambridge University Press) pp 263–78
[4] Greeley R, Wilson G, Coquilla R, White B and Haberle R T 2000 Windblown dust on Mars: laboratory simulations of flux as a function of surface roughness *Planet. Space Sci.* **48** 1349
[5] Blake D F *et al* and (the MSL Science Team) 2013 Curiosity at Gale crater, Mars: characterization and analysis of the rocknest sand shadow *Science* **341** 1239505
[6] Allen C C, Jager K M, Morris R V, Lindstrom D J, Lindstrom M M and Lockwood J P 1998 Martian soil simulant available for scientific, educational study *EOS Trans. Am. Geophys. Union* **79** 405
[7] http://phys.org/news/2015-11-devils-seismometer-Mars-mission.html
[8] Smith P H *et al* 1997 Results from the Mars Pathfinder camera *Science* **278** 1758
[9] Landis G A and Jenkins P P 2000 Measurement of the settling rate of atmospheric dust on Mars by the MAE instrument on Mars Pathfinder *J. Geophys. Res.* **105** 1855
[10] Ferguson D C, Kolecki J C, Siebert M W, Wilt D M and Matijevic J R 1999 Evidence for Martian electrostatic charging and abrasive wheel wear from the Wheel Abrasion Experiment on the Pathfinder Sojourner Rover *J. Geophys. Res.* **104** 8747
[11] Schuerger A C, Golden D C and Ming D W 2012 Biotoxicity of Mars soils: I. Dry deposition of analog soils on microbial colonies and survival under Martian conditions *Planet. Space Sci.* **72** 91
[12] Sternovsky Z, Robertson S, Sickafoose A, Colwell J and Horanyi M 2004 Contact charging of lunar and Martian dust simulants *J. Geophys. Res.* **107** 15-1–8
[13] Madsen M B, Hviid S F, Gunnlaugsson H P, Knudsen M, Goetz W, Pedersen C T, Dinesen A R, Mogensen C T, Olsen M and Hargraves R B 1999 The magnetic properties experiments on Mars Pathfinder *J. Geophys. Res.* **104** 8761
[14] Sabri F, Marchetta J G, Sinden-Redding M, Habenicht J J, Chung T P, Melton C N, Hatch C J and Lirette R L 2012 Effect of surface plasma treatments on the adhesion of Mars JSC 1 simulant dust to RTV 655, RTV 615, and Sylgard 184 *PLoS One* **7** e45719
[15] Landis G A 1998 Mars dust removal technology *J. Propulsion Power* **14** 126
[16] Goree J and Sheridan T E 1992 Particulate release from surfaces exposed to a plasma *J. Vac. Sci. Technol.* A **10** 3540
[17] Flanagan T M and Goree J 2006 Dust release from surfaces exposed to plasma *Phys. Plasmas* **13** 123504
[18] Calle C I, Buhler C R, Johansen M R, Hogue M D and Snyder S J 2011 Active dust control and mitigation technology for lunar and Martian exploration *Acta Astron.* **69** 1082
[19] Atten P, Pang H L and Reboud J-L 2009 Study of dust removal by standing-wave electric curtain for application to solar cells on Mars *IEEE Trans. Ind. Appl.* **45** 75
[20] Sharma R, Wyatt C A, Zhang J, Calle C I, Mardesich N and Mazumder M K 2009 Experimental evaluation and analysis of electrodynamic screen as dust mitigation technology for future Mars missions *IEEE Trans. Ind. Appl.* **45** 591
[21] Calle C I, Mackey P J, Hogue M D, Johansen M R, Kelley J D, Phillips J R III and Clements J S 2013 An electrostatic precipitator system for the Martian environment *J. Electrostat.* **71** 254
[22] Davis K, Herman J, Maksymuk M, Wilson J, Chu P, Burke K, Jandura L and Brown K 2012 Mars science laboratory's dust removal tool *Proc. Aerospace Mechanisms Symp. (Jet Propulsion Laboratory)* p 279 NASA/CP-2012-217653
[23] Barlow N 2008 *Mars: An Introduction to its Interior, Surface and Atmosphere* (Cambridge: Cambridge University Press)
[24] http://photojournal.jpl.nasa.gov/jpeg/PIA20012.jpg
[25] Hsu S C *et al* 2012 Spherically imploding plasma liners as a standoff driver for magnetoinertial fusion *IEEE Trans. Plasma Sci.* **40** 1287
[26] Schoenberg K, Gerwin R, Barnes C, Henins I, Mayo R, Moses R Jr., Scarberry R and Wurden G 1991 Coaxial plasma thrusters for high specific impulse propulsion *AIAA/NASA/OAI Conf. on Advanced SEI Technologies (Cleveland, OH)* AIAA Paper 91-3570
[27] Choueiri E Y 2009 New dawn for electric rocket *Sci. Am.* **300** 58
[28] Ticos C M, Wang Z, Wurden G A, Kline J L, Montgomery D S, Dorf L A and Shukla P K 2008 Plasma drag acceleration of a dust cloud to hypervelocities *Phys. Rev. Lett.* **100** 155002

[29] Ticos C M, Jepu I, Lungu C P, Chiru P, Zaroschi V and Lungu A M 2010 Removal of floating dust in glow discharge using plasma jet *Appl. Phys. Lett.* **97** 011501
[30] Wang Z, Ticos C M, Dorf L A and Wurden G A 2006 Micro-particle probes for laboratory plasmas *IEEE Trans. Plasma Sci.* **34** 242
[31] Bogatu I N, Galkin S A and Kim J S 2009 C60-fullerene hyper-velocity high-density plasma jets for MIF and disruption mitigation *J. Fusion Energy* **28** 144
[32] Manning H L K, ten Kate I L, Battel S J and Mahaffy P R 2010 Electric discharge in the Martian atmosphere, Paschen curves and implications for future missions *Adv. Space Res.* **46** 1334–40
[33] Hackam R 1969 Total secondary ionization coefficients and breakdown potentials of hydrogen, methane, ethylene, carbon monoxide, nitrogen, oxygen and carbon dioxide between mild steel coaxial cylinders *J. Phys. B: At. Mol. Phys.* **2** 216
[34] Gatsonis N A, Byrne L T, Zwahlen J C, Pencil E J and Kamhawi H 2004 Current-mode triple and quadruple Langmuir probe methods with applications to flowing pulsed plasmas *IEEE Trans. Plasma Sci.* **32** 2118
[35] Qayyum A, Ahmad N, Ahmad S, Deeba F, Ali R and Hussain S 2013 Time-resolved measurement of plasma parameters by means of triple probe *Rev. Sci. Instrum.* **84** 123502
[36] Ticos C M, Scurtu A, Toader D and Banu N 2015 Experimental demonstration of Martian soil simulant removal from a surface using a pulsed plasma jet *Rev. Sci. Instrum.* **86** 033509
[37] Haberle R M, McKay C P, Pollack J B, Gwynne O E, Atkinson D H, Appelbaum J, Landis G A, Zurek R W and Flood D J 1993 Atmospheric effects on the utility of solar power on Mars *Resources of Near-Earth Space* (*Space Science Series*) ed J S Lewis *et al* (Tucson, AZ: The University of Arizona Press) pp 845–85
[38] Dietz D 1987 Coaxial plasma accelerator in the snow plow mode: analytical solution in the weak coupling limit *J. Appl. Phys.* **62** 2669
[39] Ticos C M, Toader D, Scurtu A, Chereches T and Lixandru P 2014 Dust removal from surfaces in a low pressure environment *Proc. 41st EPS Conf. Plasma Physics (Berlin, 23–27 June)* O4J105-1/4
[40] Loebner K T K, Underwood T C and Cappelli M A 2015 Evidence of branching phenomena in current-driven ionization waves *Phys. Rev. Lett.* **115** 175001
[41] Draine B T and Salpeter E E 1979 On the physics of dust grains in hot gas *Astrophys. J.* **231** 77
[42] Tang X-Z and Delzanno G L 2014 Orbital-motion-limited theory of dust charging and plasma response *Phys. Plasmas* **21** 123708